Proceedings of the ASME 2022
International Design Engineering Technical Conferences and
Computers and Information in Engineering Conference
IDETC-CIE2022
August 14-17, 2022, St. Louis, Missouri

DETC2022-88415

CONSIDERATIONS FOR THE TESTING AND VALIDATION OF A MOBILE DAMPING ROBOT FOR OVERHEAD POWER LINES

Andrew Choi, Paul-Camille Kakou, Oumar Barry*
Department of Mechanical Engineering
Virginia Polytechnic Institute and State University
Blacksburg, Virginia 24061

ABSTRACT

While analyses have been performed for fixed masses on power line conductors, they have not been in the context of interactions between the conductor and a mobile damping robot (MDR). There is a need to explore the potential impact of the MDR on the power line and the resulting implications for the MDR's development as current methods of vibration control do not adequately address fatigue failure caused by wind-induced vibrations (WIV). Fixed passive vibration absorbers (FPVAs) are widely used on power lines, but they are inherently limited by their fixed nature since changes in wind conditions affect absorber performance as conductor mode shapes change. An MDR can overcome these limitations by actively transporting a passive absorber to conductor antinodes where the absorbers can most effectively remove energy from the system. In this paper, we experimentally investigate the effects of an untuned suspended mass on the conductor as an analog for the MDR, and we perform numerical analysis in MATLAB using equations of motion obtained via Hamilton's Principle. The insights gained from this work lay a foundation to guide future experiments that will better define the operating conditions of the MDR and lead to the creation of an appropriate control framework.

Keywords: vibration, vibration control, mobile robots

1 INTRODUCTION

Power transmission is critical to the nation's infrastructure, and its maintenance is a key priority, especially as the electric grid ages. However, up-to-date solutions do not adequately protect against structural damages caused by wind blowing across the conductor, exciting it, and causing it to vibrate. These wind-induced vibrations (WIV) are typically Aeolian vibrations in the range of 3-150 Hz caused by wind speeds of 1-7 m/s [1–7]. Over time, WIV can cause fatigue failure due to high cycles of bending stress [8–13]. Fixed passive vibration absorbers (FPVAs) exist to damp transmission line vibrations, thereby reducing amplitude in an effort to keep the cable below its endurance limit. [14–17]. However, FPVAs are fundamentally inefficient at certain resonance frequencies due to their inability to change location. In fact, if the FPVA is fixed at a node, it is theoretically worse than having no absorber at all due to the increased strain caused by the mass of the absorber [18, 19]. Although the odds of a fixed absorber's placement coinciding with the location of a node are low, the potential damage is quite high. Even low frequency vibrations for just minutes each day would result in several mega-cycles each year.

Absorbers are most effective at removing energy from the cable when they are at the location of an antinode, or position of highest amplitude. However, given their fixed nature, absorbers are rarely at these optimal locations. To overcome this shortcoming, Barry et al [13, 20–22] have proposed a novel mobile damping robot (MDR) for vibration control, as shown in Figure 1. While other mobile power line robots have been developed, they suffer from significant drawbacks. For example, their high cost, heavy weight, and need for user input causes them to be unsuitable for long-term mounting on transmission lines. Moreover, these robots focus almost exclusively on inspection rather than active control and monitoring. The MDR fills this technol-

*Corresponding Author (Email: obarry@vt.edu)

ogy gap and is specifically designed for long-term mounting and autonomous suppression of cable vibrations.

FIGURE 1: Conceptual design model of the mobile damping robot.

Therefore, a critical research need exists to examine how the presence of the MDR itself affects conductor vibrations and behavior, as well as the MDR's ability to adapt to shifting wind conditions. In this paper, we first model the cable as an Euler-Bernoulli beam with an attached spring-mass-damper. Then, we define the experimental setup and key testing parameters. Numerical methods are employed on the basis of the mathematical model and their solutions are compared to experimental results. Finally, we discuss our findings and suggestions for future improvements and experiments to better develop the MDR.

2 MATHEMATICAL FORMULATION

A mathematical model of the system is used for analysis in MATLAB [20, 22–25]. The cable and untuned mass are modeled as forced vibration of a mass-spring-damper-mass system as depicted in Figure 2. Here, x is the horizontal placement of the mass on the cable span, m_i is the in-span mass of the clamp, k is the spring constant, c is the damping constant, m_d is the suspended mass, and y_d is the vertical displacement of the suspended mass. Horizontal displacement is set to be zero, and self-damping is considered to be minimal. The cable is modeled as an Euler-Bernoulli beam to better capture the system's behavior, and the cable's parameters are summarized in Table 1.

The position vectors of the beam, in-span mass, and suspended mass are first defined to represent their positions and displacements. The time derivatives of the position vectors are then derived and used to further derive the velocity vectors. The velocity vectors are used to find the kinetic energy of the system elements, the sum of which define the kinetic energy of the system as a whole. The potential energy is defined for the system elements with consideration of restoring forces. The application of Hamilton's Principle to these equations results in the following

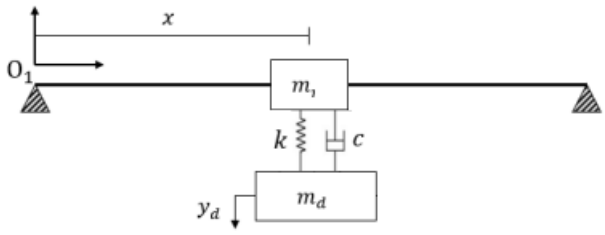

FIGURE 2: Schematic of a single conductor with a suspended mass.

TABLE 1: Cable Parameters.

Parameter	Value	
Mass	m	0.68 kg
Length	L	3.66 m
Tension	T	395 N
Diameter	d	1.05 x10^{-2} m
Flexural Rigidity	EI	40.8 m^4

equation of motion

$$EIy'''' + m\ddot{y} + Ty'' = F(x,t) - (F_1 + F_2)D(x,t) \tag{1}$$

Here $F(x,t)$ is an excitation force at a single point expressed in the form of

$$F(t) = f_0 sin(\omega_e t) \tag{2}$$

where f_0 is the amplitude of the force, and ω_e is the input frequency. F1, F2 and D(x,t) are expressed as

$$F_1 = m_d\ddot{y} \tag{3}$$

$$F_2 = k(y - y_d) + c(\dot{y} - \dot{y_d}) \tag{4}$$

$$D(x,t) = \delta(x - x_r) \tag{5}$$

Finally, the transverse displacement of the suspended mass is given to be

$$m_d\ddot{y}_d - F_2 = 0 \tag{6}$$

3 EXPERIMENTS

The experiments were performed using an exciter (LDS Test and Measurement V408 electrodynamic shaker), an analyzer (Siemens SCADAS Mobile), and a signal conditioner (Bruel & Kjaer LDS LPA100 amplifier) as depicted in Figure 3. Additionally, an accelerometer (PCB Piezotronics 352C33) was used to measure the input acceleration of the shaker as a reference with another accelerometer (PCB Piezotronics YT352C34) placed at an antinode of the mode shape corresponding to the forcing frequency. Siemens Simcenter Testlab software was used to interface with the hardware and record data.

FIGURE 3: Experiment hardware. (1) exciter, (2) analyzer, (3) signal conditioner.

Figure 4 depicts a schematic of the experimental setup, which entailed securing the cable to two towers using p-clamps and two-hole straps. A Haul-Master hand winch was used to tension the cable to 395 N, as measured using a PCE-CS 300 force gauge. The tensioning and excitation portions of the setup are depicted in Figure 5. The towers were composed of slotted aluminum angles, and the cable was an Aster All Aluminum Conductor (AAC) with a diameter of 1.05 cm. The cable span was 3.66 m, and the shaker was attached to the cable at midspan.

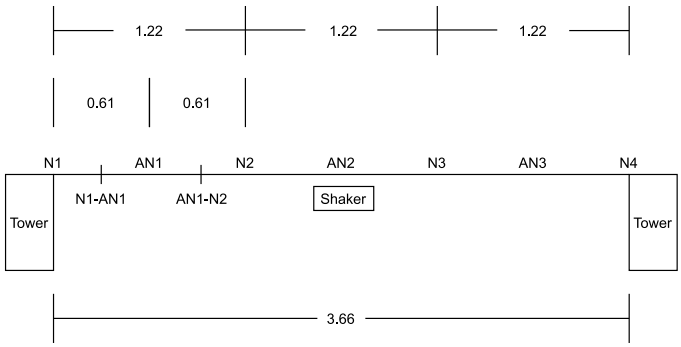

FIGURE 4: Diagram of the experimental setup. All dimensions are in meters. N = node, AN = antinode. Locations between a node and antinode are denoted with a dash.

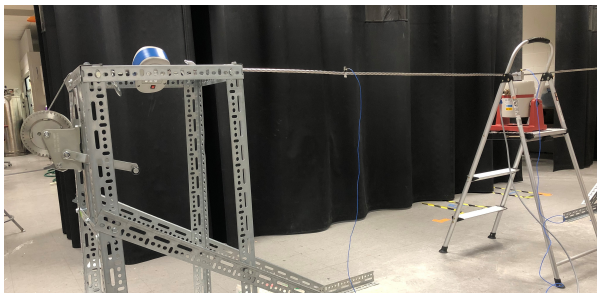

FIGURE 5: Experimental setup. The right non-tensioning tower is to the right of frame.

A stepped sine output was used to obtain the frequency response of the cable across a range of 10 - 25 Hz with a step increment of 0.01 Hz. Resonance in the frequency response function was best seen at the second mode shape around 12.6 Hz, which was verified by visual observation of the cable. This response suggested a fundamental frequency of 6.3 Hz. When evaluated at a forcing frequency of 18.9 Hz, the cable was vibrating at high amplitude and clearly demonstrated a third mode shape. The third mode was selected for the experiment since it best fit the constraints of the experimental setup. The loop lengths were found to be equal at 1.22 m per loop for each of three loops across the 3.66 ft span.

The fundamental frequency was verified to align with the theoretical value given by

$$f_n = \frac{1}{2L}\sqrt{\frac{T}{\rho A}} \tag{7}$$

where L is length of the cable span (3.66 m), T is the tension of the cable (395 N), and ρA is the mass per unit length (0.186 kg/m). The theoretical fundamental frequency was 6.3 Hz indicating a theoretical third mode at 18.9 Hz, which matched the selected forcing frequency for the experiment.

Initially, the cable alone was tested with a sine output. The response of the cable was displayed as a time series in Testlab with real acceleration on the y-axis in m/s^2. Acceleration values were automatically adjusted to account for offset due to gravity so that 9.8 m/s^2 was equal to 0. After data collection, the maximum accelerations were determined and plotted in Figure 6. As expected, the acceleration at the nodes was near zero, and the acceleration was highest at the antinode.

Next, the mass corresponding to 5% of the cable mass was hung between the first node (tower-cable connection) and antinode of the first vibration loop of the cable. Acceleration data was collected at 0.305 m increments from the first node to the second

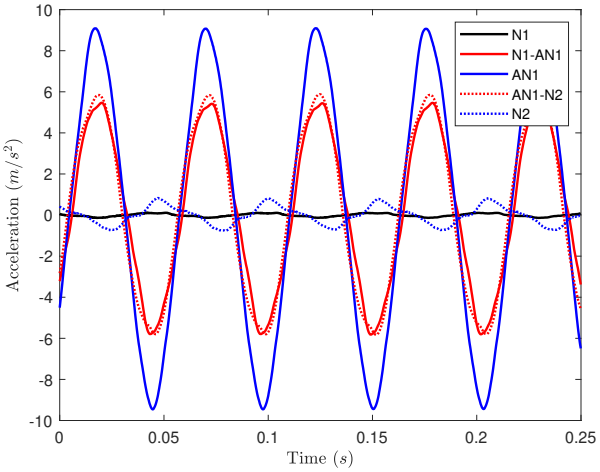

FIGURE 6: Acceleration values for the cable without any mass attached. Locations midway between nodes and the antinode are denoted with a dash. E.g., the position halfway between node 1 (N1) and antinode 1 (AN1) is defined as N1-AN1.

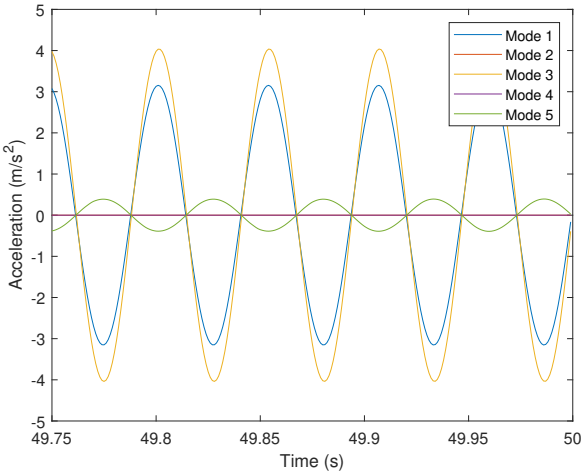

FIGURE 7: Acceleration for each composite mode of the cable's steady state response.

node, for a total of five measurement locations. Then the mass was moved in 0.305 m increments to the second node for a total of four suspension locations. This resulted in a total of 20 data points per mass. This process was also completed for the 10%, 15%, 20%, and 25% masses for a total of 100 data points. The masses used are defined in Table 2.

TABLE 2: Values of masses used.

Target %	**5%**	**10%**	**15%**	**20%**	**25%**
Target Mass	34g	68g	102g	136g	170g
Actual Mass	34.6g	66.7g	101.6g	140.2g	170.3g
Actual %	5.1%	9.8%	14.9%	20.6%	25.0%
% Difference	1.7%	0.4%	0.4%	3.1%	0.2%

4 RESULTS AND DISCUSSION

4.1 Numerical

MATLAB's ODE45 function was used to simulate the acceleration of the cable and suspended mass. An approximation of $n = 5$ was used, with the in-span and suspended masses independent of the number of modes. The solution for the cable alone (Figure 7) showed that the 3rd mode dominated the response, as expected for the excitation frequency used. The modes were summed, and the numerical solution showed good agreement with the experimental result, as seen in Figure 8.

Solutions were then found for the cable with the suspended masses. The masses were simulated at the first antinode and second node locations. Modeling produced decreasing acceleration in both cases. As shown in Figures 9 and 10, these results were only partially consistent with the experimental findings. The experiments demonstrated that placement of the masses at the antinode matched the numerical trend and reduced vibration, while also demonstrating the opposite trend for the mass placed at the node as acceleration actually increased experimentally. Additionally, the scale of the acceleration changes for the mass placed at the node was markedly different, with the numerical analysis producing much higher amplitudes and significantly larger changes for each increase in mass.

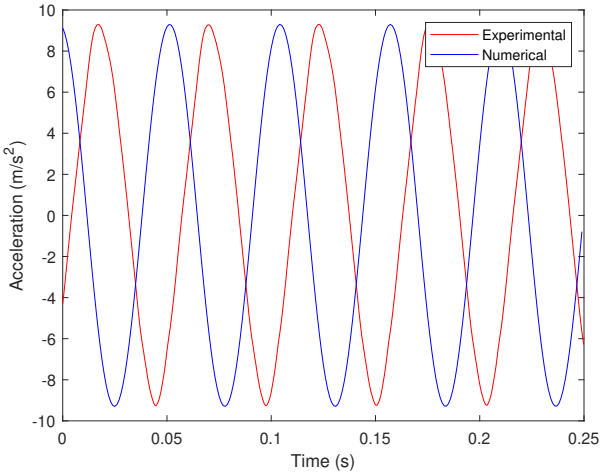

FIGURE 8: Comparison of the experimental acceleration and the summed numerical acceleration for the cable only as measured at the first antinode.

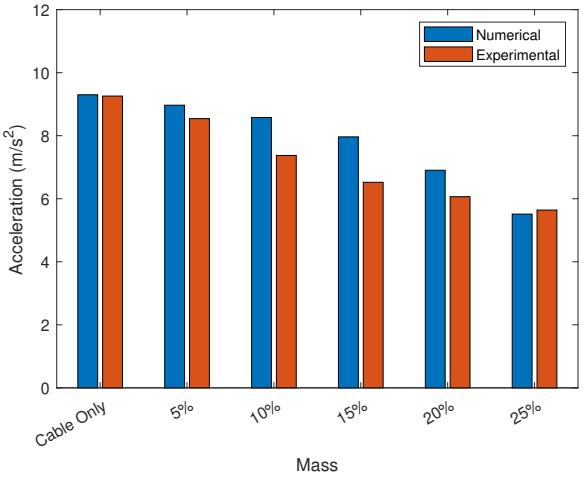

FIGURE 9: Acceleration with mass and measurement at first antinode.

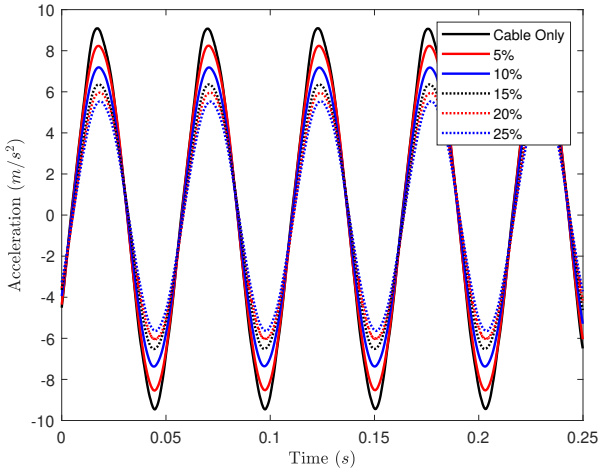

FIGURE 11: Acceleration at the antinode of the first loop when the mass was suspended at the same antinode.

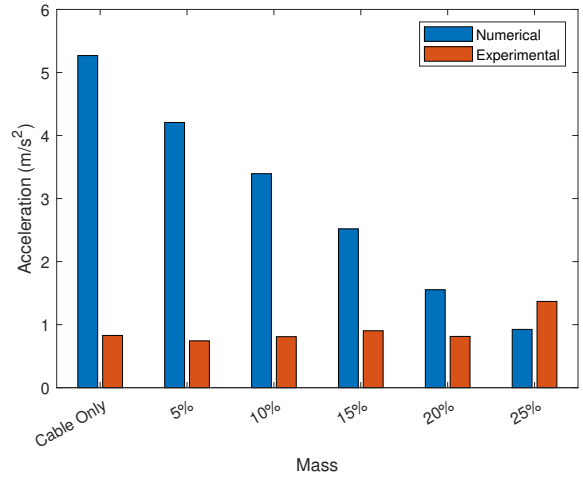

FIGURE 10: Acceleration with mass and measurement at second node.

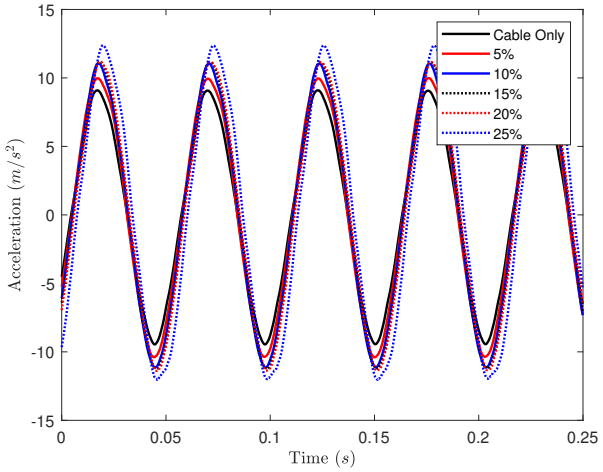

FIGURE 12: Acceleration at the antinode of the first loop when the mass was suspended from the position of the second node.

4.2 Experimental

The rest of the experimental data confirmed the relationship between the numerical and experimental results. The experiments demonstrated that the addition of mass had a clear positive effect on cable vibration when placed at the antinode and had a clear negative effect when placed at the node. Figures 11 and 12 show the acceleration at the antinode with masses at those two locations.

We also observed that the addition of a mass to the vibration loop caused the second node to shift inward toward the antinode, which aligned with numerical findings. Each increase in mass corresponded to an increasing leftward movement of the node toward the antinode, demonstrating a shrinking vibration loop length dependent on suspended mass. The total movement in cm was greater at lower masses with less movement at higher masses. This indicates that there may be a rough limit to the shortening effect with mass increases above 25% likely causing convergence toward a minimum loop length.

Figure 13 shows the amount by which the vibration loop shrunk when the masses were placed at the antinode. The white marking indicates the original node position at 1.22 m. The yellow marking indicates the node position with the 5% mass, and

each subsequent rightward marking indicates the node position for the remaining masses in ascending order. Note that the new locations of the node indicate by how much the loop has shortened. These results are summarized in Table 3.

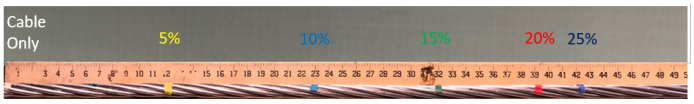

FIGURE 13: Distance by which the node shifted with addition of each mass to the cable.

TABLE 3: Node shifts. Deltas indicate the amount by which the loop length shortened due to the presence of the masses.

Mass %	Color	Delta (cm)	Delta (%)
5%	Yellow	∼12.25	∼10.0%
10%	Teal	∼23.0	∼18.9%
15%	Green	∼32.0	∼26.2%
20%	Red	∼39.25	∼32.2%
25%	Blue	∼42.25	∼34.6%

While these shifts were visually observed and recorded, it was necessary to verify the shifts by taking additional measurements at each new node location. The results of these tests can be seen in Figure 14 and demonstrate that the acceleration at each new node location aligned closely with one another and the original measurement at the node for the cable only. These accelerations were also found to be significantly reduced from those same locations for the cable alone.

Brief testing was also performed at the fifth harmonic to determine the effect of untuned masses on the vibration loops. The second loop was tested since a loop with two free nodes was of interest. While the loop lengths of the fifth harmonic were unequal, the antinodes were still found to be in the middle of their respective loops. Also, while both nodes of the loop shifted inward, they moved in unequal fashion. The node nearer to the tower moved in relatively small increments of less than 3 cm while the node nearer to midspan moved in larger increments up to 10 cm. The node nearest the midspan seemed to experience less movement with each increase in mass, whereas the node nearest the tensioning tower seemed to experience slightly more movement with each increase in mass.

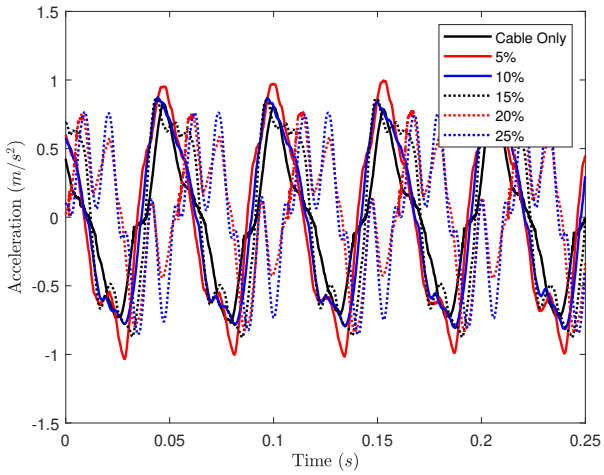

FIGURE 14: Acceleration at the new node location for each mass.

4.3 Discussion

The mathematical model did not fully reflect the experimental results. The lack of congruence in the trends and values indicates that we cannot validate the mathematical model for this experimental setup. This was despite making adjustments to model the input force as harmonic excitation of a single frequency with a single point input midspan. We will investigate more complex models that account for nonlinear effects and other considerations since there was significant deviation between the experimental results and what was predicted by the numerical analysis for the node case. Altering the mathematical model to simulate a uniformly distributed wind force composed of various frequencies and comparing to experiments in a wind tunnel or field environment may return more consistent results. Measures for improving the experimental test bench are outlined below.

Due to the relatively narrow scope of untuned masses on a short cable span at a single resonance frequency, there were limitations to this study that offer opportunities for future experiments. For example, the cable used here was relatively lightweight and short. Although the measurement accelerometer and its clamp totaled a modest 8.65 g, and the width of the clamp was just 0.95 cm, they could have interfered with the cable's frequency response. Additionally, since the node should theoretically be a single cross-sectional slice of the cable, it was impossible to mount an accelerometer over its exact location. This resulted in variation of acceleration values at the node based on the accelerometer's placement. A larger diameter cable could mitigate these unintended effects since the accelerometer's mass would be a lower proportion of the cable mass and the clamp's contact area would be a lower proportion of the cable length.

Another aspect that that may have impacted the data is the collection of measurements from a terminal loop adjacent to a tower. With excitation corresponding to the third mode shape, testing on the middle span was not feasible due to the placement of the shaker. The impact of the masses on cable vibration may have been modified by proximity to the tower. While additional testing was attempted on a non-terminal loop at a higher order mode shape, the short cable span made it difficult to observe the effects on the cable, let alone properly measure them. Therefore, there are opportunities for future testing with a longer cable.

5 CONCLUSION

The numerical analysis demonstrated that cable vibrations improve when an untuned mass is suspended from the cable at both antinode and node locations with the impact increasing with increasing mass. The experiments showed partial agreement with the numerical analysis, verifying that suspending an untuned mass at the location of an antinode improves vibration while contradicting the result that suspending a mass at the location of a node improves vibration. In the latter case, the opposite was found, wherein the masses worsened vibrations along the cable. Experimental findings also verified the shrinking of loop lengths seen numerically.

We conclude that additional considerations must be made for how the MDR will affect conductor dynamics and for future testing and validation of a physical MDR prototype beyond the experimental setup used in this paper. These findings will assist the development of the MDR by guiding development of a more versatile test bench, proper shaker placement, and providing input for control algorithms. In particular, these results will inform how the MDR will operate when the cable resonates at a frequency for which the absorbers are not tuned. Moreover, it lays the groundwork for future experiments with tuned masses to assess how the cable response changes.

ACKNOWLEDGMENTS

This work is funded by National Science Foundation CAREER Award ECCS 1944032: Towards a Self-Powered Autonomous Robot for Intelligent Power Lines Vibration Control and Monitoring. Any opinions, findings, and conclusions or recommendations expressed in this material are those of the author(s) and do not necessarily reflect the views of the National Science Foundation.

REFERENCES

[1] Oumar Barry, Donatus CD Oguamanam, and Der Chyan Lin. Aeolian vibration of a single conductor with a stockbridge damper. *Proceedings of the Institution of Mechanical Engineers, Part C: Journal of Mechanical Engineering Science*, 227(5):935–945, 2013.

[2] Morteza Sadeghi and Aryo Rezaei. Aeolian vibrations of transmission line conductors with more than one damper. *International Journal of Engineering*, 28(10):1515–1524, 2015.

[3] Kunpeng Ji, Bin Liu, Jingchao Wang, Peng Li, Danyu Li, Lichun Zhang, Jingshan Han, and Yifeng Wang. Aeolian vibration and its suppression methods of long crossing span overhead electric transmission line. In *2019 6th International Conference on Information Science and Control Engineering (ICISCE)*, pages 663–667. IEEE, 2019.

[4] Rafiou Oumar Barry. *Vibration Modeling and Analysis of a Single Conductor With Stockbridge Dampers*. PhD thesis, University of Toronto, 2014.

[5] Suzanne Guerard, Bertrand Godard, and Jean-Louis Lilien. Aeolian vibrations on power-line conductors, evaluation of actual self damping. *IEEE transactions on power delivery*, 26(4):2118–2122, 2011.

[6] O Barry, JW Zu, and DCD Oguamanam. Analytical and experimental investigation of overhead transmission line vibration. *Journal of Vibration and Control*, 21(14):2825–2837, 2015.

[7] Chiara Gazzola, Francesco Foti, Luca Martinelli, and Federico Perotti. An appraisal of modelling strategies for assessing aeolian vibrations of transmission lines. In *24th Conference of the Italian Association of Theoretical and Applied Mechanics, AIMETA 2019*, pages 1522–1534. Springer, 2020.

[8] GE Braga, R Nakamura, and TA Furtado. Aeolian vibration of overhead transmission line cables: endurance limits. In *2004 IEEE/PES Transmision and Distribution Conference and Exposition: Latin America (IEEE Cat. No. 04EX956)*, pages 487–492. IEEE, 2004.

[9] YD Kubelwa, RC Loubser, and P Moodley. Experimental investigations of bending stresses of acsr conductors due to aeolian vibrations. In *Cigre Science & Engineering*, volume 9, pages 1286–1146. Innovation in the power systems industry, 2017.

[10] Suzanne Guérard, Jean-Louis Lilien, et al. Evaluation of power line cable fatigue parameters based on measurements on a laboratory cable test span. In *EIght International symposium on Cable Dynamics, ISCD 2009*, page 125. AIM, rue St Gilles, 31, 2009.

[11] CBSInternational Journal of Mechanical Sciences. 4,000 dte customers remain without power nearly a week after damaging winds. 1:163–178, 2017.

[12] President's Council of Economic Advisers. Economic benefits of increasing electric grid resilience to weather outages. 1:163–178, 2013.

[13] Oumar Barry and Mohammad Bukhari. On the modeling and analysis of an energy harvester moving vibration absorber for power lines. In *Dynamic Systems and Control Conference*, volume 58288, page V002T23A005. American Society of Mechanical Engineers, 2017.

[14] NK Vaja, OR Barry, and EY Tanbour. On the modeling and analysis of a vibration absorber for overhead powerlines with multiple resonant frequencies. *Engineering Structures*, 175:711–720, 2018.

[15] Oumar Barry, JW Zu, and DCD Oguamanam. Nonlinear dynamics of stockbridge dampers. *Journal of Dynamic Systems, Measurement, and Control*, 137(6):061017, 2015.

[16] Nitish Kumar Vaja, Oumar Barry, and Brian DeJong. Finite element modeling of stockbridge damper and vibration analysis: Equivalent cable stiffness. In *International Design Engineering Technical Conferences and Computers and Information in Engineering Conference*, volume 58226, page V008T12A012. American Society of Mechanical Engineers, 2017.

[17] Oumar Rafiou Barry, Emadeddin Y Tanbour, Nitish Kumar Vaja, and Hesham Tanbour. Asymmetric aeolian vibration damper, April 17 2018. US Patent 9,948,081.

[18] A Rezaei and MH Sadeghi. Analysis of aeolian vibrations of transmission line conductors and extraction of damper optimal placement with a comprehensive methodology. *International Journal of Engineering*, 32(2):328–337, 2019.

[19] ML Lu and JK Chan. An efficient algorithm for aeolian vibration of single conductor with multiple dampers. *IEEE Transactions on power Delivery*, 22(3):1822–1829, 2007.

[20] Paul Kakou, Mohammad Bukhari, Jiamin Wang, and Oumar Barry. On the vibration suppression of power lines using mobile damping robots. *Engineering Structures*, 239:112312, 2021.

[21] Paul-Camille Kakou. *Towards A Mobile Damping Robot For Vibration Reduction of Power Lines*. PhD thesis, Virginia Tech, 2021.

[22] Paul-Camille Kakou and Oumar Barry. Toward a mobile robot for vibration control and inspection of power lines. *ASME Letters in Dynamic Systems and Control*, 2(1):011001, 2021.

[23] O Barry, R Long, and DCD Oguamanam. Simplified vibration model and analysis of a single-conductor transmission line with dampers. *Proceedings of the Institution of Mechanical Engineers, Part C: Journal of Mechanical Engineering Science*, 231(22):4150–4162, 2017.

[24] O Barry, JW Zu, and DCD Oguamanam. Forced vibration of overhead transmission line: analytical and experimental investigation. *Journal of Vibration and Acoustics*, 136(4), 2014.

[25] Mohammad A Bukhari and Oumar R Barry. Nonlinear vibrations analysis of overhead power lines: A beam with mass–spring–damper–mass systems. *Journal of Vibration and Acoustics*, 140(3), 2018.